PSFC/JA-01-28

Equilibrium and Confinement of Bunched Annular Beams

M. Hess and C. Chen

December 2001

Plasma Science and Fusion Center
Massachusetts Institute of Technology
Cambridge, MA 02139, USA

This work was supported by the Air Force Office of Scientific Research, Grant No. F49620-00-1-0007, and the Department of Energy, Office of High Energy and Nuclear Physics, Grant No. DE-FG02-95ER-40919. Reproduction, translation, publication, use and disposal, in whole or part, by or for the United States government is permitted.

Submitted for publication in *Physics of Plasmas.*

Equilibrium and confinement of bunched annular beams

Mark Hess and Chiping Chen
Plasma Science and Fusion Center
Massachusetts Institute of Technology
Cambridge, MA 02139

ABSTRACT

The azimuthally invariant cold-fluid equilibrium is obtained for a periodic, strongly bunched charged annular beam with an arbitrary radial density profile inside of a perfectly conducting cylinder and an externally applied uniform magnetic field. The self-electric and self-magnetic fields, which are utilized in the equilibrium solution, are computed self-consistently using an electrostatic Green's function technique and a Lorentz transformation to the longitudinal rest frame of the beam. An upper bound on the maximum value of an effective self-field parameter for the existence of a bunched annular beam equilibrium is obtained. As an application of the bunched annular beam equilibrium theory, it is shown that the Los Alamos National Laboratory relativistic klystron amplifier experiment is operating slightly above the effective self-field parameter limit, and a discussion of why this may be the cause for their observed beam loss and microwave pulse shortening is presented. The existence of bunched annular beam equilibria is also demonstrated for two other high-power microwave (HPM) experiments, the relativistic klystron oscillator experiment at Air Force Research Laboratory and the backward wave oscillator experiment at the University of New Mexico. In general, the results of the equilibrium analysis will be useful in the determination of the stability properties of strongly bunched annular beams in HPM devices.

PACS: 29.27, 41.85

I. INTRODUCTION

In recent years, a number of high-power microwave (HPM) experiments have employed high-intensity bunched annular relativistic electron beams, such as the relativistic klystron amplifier (RKA) experiment at Los Alamos National Laboratory (LANL) [1], relativistic klystron oscillator (RKO) experiment at Air Force Research Laboratory (AFRL) [2], and the backward wave oscillator (BWO) at the University of New Mexico [3]. Since an annular beam typically has a transverse size, which is of the order of the conductor wall radius, the beam-wall interaction can be increased compared to the interaction of a pencil beam with a wall. The greater beam-wall interaction can advantageously provide a higher power microwave source. However, the increase in beam-wall interaction, especially when the beam becomes strongly bunched during high-power operation of such a device, may require a stronger magnetic field for beam focusing. Indeed, many HPM devices driven by annular beams suffer from considerable beam losses and the well-known problem of rf pulse shortening [1,3].

In previous papers [4,5], the authors had success in using a Green's function technique for modeling a strongly bunched pencil beam with negligibly small transverse size. A constraint was found on the maximum effective self-field parameter, $2w_p^2/w_c^2$, which is a measure of the space charge in the beam for a given magnetic field strength. In the previous expression, w_p is the effective plasma frequency and w_c is the electron cyclotron frequency. This parameter limit agreed well with the self-field parameters of three periodic permanent magnet (PPM) klystron experiments, i.e., 50 MW-XL PPM [6,7], 75 MW-XP [6,7] and the Klystrino [8], which are all at the Stanford Linear Accelerator Center.

In this paper, we will examine the constraints on the maximum effective self-field parameter for a bunched annular beam with negligibly small longitudinal thickness in a perfectly conducting cylindrical pipe. The limit, which we will analyze in this paper, pertains to the equilibrium transport of the bunched annular beam with no beam loss in the pipe. Unlike the well-known space-charge limiting current, which was derived under the assumption of an infinitely strong axial guide magnetic field and an unbunched (continuous) beam [9], the present limit applies to a bunched beam in a finite axial guide magnetic field. In particular, we develop a relativistic traveling-wave equilibrium fluid

theory to model the transverse density distribution of the strongly bunched annular beam. The electric field inside of the beam is completely self-consistent, i.e., the electric field includes contributions from the beam and the induced surface charge on the conductor wall. It is obtained through a Green's function technique.

By using density test functions to compute the maximum self-field parameters for annular beams, we compare theoretical parameter limits with those corresponding to three annular beam experiments – 1.3 GHz RKA experiment at LANL [1], 1.3 GHz RKO [2] experiment at AFRL, and the 9.4 GHz BWO [3] experiment at the University of New Mexico. We note that the density functions used for modeling these experiments are in fluid equilibrium, but their stability is still unknown at the moment and will be studied in our future research. By performing a stability analysis involving radial and azimuthal perturbations on the beam equilibrium, one may find a lower value on the maximum self-field parameter than what the cold-fluid equilibrium theory predicts.

In an earlier paper [10], Prasad and Morales explored the equilibrium and wave properties of two-dimensional ion plasmas of finite temperature, T, inside of a pillbox conductor geometry. The plasma equilibrium was established by balancing the plasma pressure and the self-electric field, calculated from Poisson's equation, with an externally applied electric field due to the fixed potential walls of the conductor. They analyzed the wave attributes of the plasma in both the unmagnetized and magnetized cases, and discussed the plasma equilibrium in the cold plasma limit, i.e., $T \to 0$. However, in their analysis of the magnetized case, they treated the angular fluid velocity of the plasma as a perturbed quantity, and assumed that the equilibrium fluid velocity is zero. In a later paper [11], Prasad and Morales analyzed the rigid-rotor equilibrium for a two-dimensional ion plasma in the cold limit with an external magnetic field present. This model was assumed to be in free space, and hence, the effects of the conductor wall were not included. The equilibrium fluid analysis in our paper includes, the self-consistent treatment of the electric fields in the presence of the conducting wall, magnetic field confinement, and the non-zero angular fluid velocity of the beam. Unfortunately, there is no regime in which we can compare the present analysis with the earlier analyses in Refs. 10 and 11.

The paper is organized in the following manner. In Sec. II, we discuss the self-consistent cold-fluid periodic bunched annular beam equilibrium model with arbitrary transverse density profile. This presentation includes the self-consistent profiles for the self-electric and self-magnetic fields generated by the beam, the equilibrium fluid rotational profile of the beam, and a constraint on the maximum self-field parameter given the previously mentioned profiles. The derivations of the self-electric and self-magnetic fields from a Green's function technique are given in the Appendix. In Sec. III, we demonstrate how the annular beam equilibrium model can be implemented numerically, which is necessary for modeling the annular beams of actual experiments. Specifically, we discuss how to numerically solve for the relevant profiles mentioned in Sec. II, and obtain a numerical result for the maximum self-field parameter. We then apply the model three HPM experiments at the LANL, AFRL, and the University of New Mexico in Sec. IV. A summary and concluding remarks are provided in Sec. V.

II. TRAVELING-WAVE RELATIVISTIC EQUILIBRIUM MODEL

The charged particle beams utilized in high-power microwave devices, such as the RKA, RKO, and the BWO, will be longitudinally bunched in order to release energy to the output cavity. Although, the beam will still have finite longitudinal thickness after bunching, in the case of an annular beam, the transverse size may become comparable to the longitudinal size. In general, modeling a bunched beam self-consistently with finite thickness requires a fully three-dimensional numerical calculation, which the authors are currently pursuing. In order to incorporate the bunching phenomenon into a partial analytical model, we will simplify the system by treating the annular bunched relativistic electron beam to be a series of charged disks spaced by a distance, L, with zero longitudinal thickness. Each disk represents a bunch of charge that has an equilibrium fluid velocity,

$$\mathbf{V}(\mathbf{r},t) = V_r(r)\hat{\mathbf{e}}_r + V_q(r)\hat{\mathbf{e}}_q + V_z\hat{\mathbf{e}}_z, \tag{1}$$

inside of a grounded perfectly conducting cylindrical pipe of radius, a. The z-axis is chosen to be the axis of the cylinder, and we only analyze azimuthally invariant charge distributions. The azimuthally invariant assumption is a major simplification of the present fluid analysis that still allows for an equilibrium distribution in the beam. Although azimuthal variations in annular intense relativistic electron beams that lead to beam-breakup instabilities are known to exist [12], we ignore these types of variations in our analysis. We include a constant external magnetic field, $\mathbf{B} = B_0\hat{\mathbf{e}}_z$, for beam focusing. Figure 1 illustrates the model.

In general, the bunch distribution has radial dependence, and can be written as,

$$n(\mathbf{r},t) = N_b s(r) \sum_{k=-\infty}^{\infty} d(z - V_z t - kL), \tag{2}$$

where N_b is the number of particles in a bunch, s contains the radial dependence in the bunch density, and d is the Dirac delta function. Equation (2) immediately yields the following normalization, $2p\int_0^a dr\, r\, s(r) = 1$. An additional assumption in our model is that the effect of finite temperature in the system may be ignored, so that the cold-fluid approximation can be made.

While in any actual HPM device there is a z-dependent velocity spread in the bunch, we have ignored this dependence in (1) to make the problem more tractable. This together with the assumption in equation (2) describes a tightly bunched beam during the full power operation of the HPM device.

Since the transverse charge distribution, s, will be a sufficiently well-behaved function, i.e., piecewise continuous in the region $0 \le r \le a$, it may be expanded in terms of Fourier-Bessel series,

$$s(r) = \sum_{m=1}^{\infty} s_m J_0(j_{0m} r/a), \tag{3}$$

where $J_l(x)$ is the lth order Bessel function of the first kind, j_{lm} is the mth positive zero of $J_l(x)$, and $\{s_m\}$ is the set of expansion coefficients.

For the traveling-wave equilibrium velocity and density profiles defined in (1) and (2) it is readily shown from the continuity equation,

$$\frac{\partial n(\mathbf{r},t)}{\partial t} + \nabla \cdot (n(\mathbf{r},t)\mathbf{V}(\mathbf{r},t)) = 0, \tag{4}$$

that $\partial(rsV_r)/\partial r = 0$. Therefore, rsV_r is a constant. Since $rsV_r\big|_{r=a} = 0$, we have $rsV_r = 0$, which implies that

$$V_r = 0 \tag{5}$$

everywhere.

In the paraxial approximation, the equilibrium force balance equation is expressed as,

$$g_b(\mathbf{V}\cdot\nabla)\mathbf{V} = -\frac{e}{m_e}\left[\mathbf{E}^{self} + \frac{\mathbf{V}}{c}\times\left(\mathbf{B}^{ext} + \mathbf{B}^{self}\right)\right], \tag{6}$$

where $\mathbf{E}^{self}$ is the self-consistent electric field due to the charge bunches and the induced charges on the conductor wall, $\mathbf{B}^{ext} = B_0\hat{\mathbf{e}}_z$ is the external focusing magnetic field, and $\mathbf{B}^{self}$ is the magnetic field associated with the longitudinal motion of the beam. Likewise, $-e$ denotes the charge of an electron, m_e is the rest mass of an electron, and c is the speed of light in a vacuum. The relativistic beam mass factor is given by $g_b \cong (1-V_z^2)^{-1/2}$, since the motion in the transverse direction is small compared to the longitudinal motion in the paraxial approximation. Note that we are implicitly assuming

that the magnetic field due to the transverse motion of the beam is much smaller than the applied field. By enforcing azimuthal symmetry, we find that $\mathbf{E}^{self} = E^{self}(r)\hat{\mathbf{e}}_r$ and $\mathbf{B} = B_0\hat{\mathbf{e}}_z + B^{self}(r)\hat{\mathbf{e}}_q$, where E^{self} and B^{self} will be derived in Appendix A and are given by,

$$E^{self} = -2pN_b e g_b \sum_{m=1}^{\infty} \hat{n}_m J_1(j_{0m} r/a)\coth(j_{0m} g_b L/2a), \tag{7}$$

$$B^{self} = \frac{V_z}{c} E^{self}. \tag{8}$$

A non-trivial solution to the equilibrium force equation is $V_z =$ constant in the beam and $V_q = V_q(r) = r w_b(r)$ satisfying the equation,

$$w_b(r) = \frac{w_c}{2g_b}\left[1 \pm \sqrt{1 + \frac{4eE^{self}}{g_b w_c^2 m_e r}}\right], \tag{9}$$

where $w_c = eB_0/m_e c$ is the non-relativistic electron cyclotron frequency. Since the argument under the square root in equation (9) must be positive, we can establish a lower bound on the internal electric field inside the beam,

$$E^{self} \geq -g_b w_c^2 m_e r/4e, \tag{10}$$

which must be satisfied everywhere $s(r) \neq 0$. It proves useful to introduce the following dimensionless self-electric field,

$$\Gamma(r) \equiv -LE^{self}(r)a^2/2rN_b e. \tag{11}$$

From (7), we immediately find that

$$\Gamma(r) = \frac{2p^2 a^3}{ar} \sum_{k=1}^{\infty} s_m J_1(j_{0m} r/a) coth(p j_{0m}/a), \tag{12}$$

where $a = 2pa/g_b L$. In order for (10) to be satisfied throughout the beam density profile, a maximum of the function $\Gamma(r)$, which we shall denote as $\Gamma_{\max}$, must exists.

In general, we can establish a space-charge limit on the beam, i.e., an upper bound on the self-field parameter, $2w_p^2/w_c^2$, where $w_p = (4pN_b e^2 n_b/m_e)^{1/2}$ and $n_b = (pa^2 g_b L)^{-1}$ are, respectively, the effective plasma frequency and effective bunch density in the rest frame of the beam. Note that when we Lorentz boost to the rest frame of the beam, the

bunch spacing becomes $L_{rest} = g_b L$. Using (10), we can express the space-charge limit in terms of the self-field parameter as

$$\frac{2w_p^2}{w_c^2} \le \frac{1}{\Gamma_{\max}}. \tag{13}$$

In the following sections, we will use equation (13) to uncover space-charge limits on strongly bunched annular beams. Once the value of $2w_p^2/w_c^2$ is chosen in the model, such that it satisfies (13), the fast and slow angular velocity profiles of the beam may be expressed as,

$$w_b(r) = \frac{w_c}{2g_b}\left[1 \pm \sqrt{1 - \frac{2w_p^2}{w_c^2}\Gamma(r)}\right], \tag{14}$$

where the plus (minus) sign denotes the fast (slow) solution to the angular velocity profile. Physically, $w_b(r)$ is only needed in the region where the beam density is non-zero. However, for reasonable choices of $s(r)$, $\Gamma(r)$ will achieve its maximum inside the beam. Combining the density and angular velocity profiles in (2) and (14), along with chosen values for a and $2w_p^2/w_c^2$, provides a closed model for a traveling-wave equilibrium beam for a bunched annular beam.

III. NUMERICAL RESULTS

In this section, we apply the fluid theory formalism to bunched annular electron beams. As discussed in the Introduction, intense annular electron beams have been used in a variety of high-power microwave experiments, such as the relativistic klystron amplifier and oscillator and the backward wave oscillator. Annular electron beams can provide a higher beam-wall interaction than an equivalent pencil electron beam, and therefore, annular beams can offer better energy efficiency in certain experiments. However, the increased beam-wall interaction may lead to beam loss or other deleterious effects.

Bunched annular beam distributions form a special class of solutions which self-consistently solve the fluid theory discussed in the previous section. We define the geometry of an annular beam bunch by an inner radius, r_i and an outer radius, r_o. Further, we assume that the beam density is zero for $r \le r_i$ and $r \ge r_o$. It is important that the radial density goes to zero sufficiently fast at the inner and outer radii, since the electric field defined by (7) will otherwise diverge near the beam edges. In order for the electric field to be finite at the edges, s must go to zero at least as fast as $\left|\ln\left|r - r_e\right|\right|^{-1}$ where r_e is either r_i or r_o. Therefore, the fluid theory does not allow the simple waterbag distribution (s = constant for $r_i \le r \le r_o$) as a solution.

In order to calculate numerically the electric field associated with a bunched annular beam, we must specify a radial density distribution. The choice of a radial density distribution, $s(r)$, for an annular electron beam needs only to satisfy the requirements of being zero at the edges and piecewise continuous. We will demonstrate numerically that the space charge limit will vary only slightly by choosing a different density function.

The two density trial functions, a quadratic function and a tent function, with which we compare the space charge limits are given by

$$s(r) = f_1(r) = \begin{cases} 0, & r \le r_i, \\ 3(r_o - r)(r - r_i)/\bar{p}\bar{r}d^3, & r_i \le r \le r_o, \\ 0, & r_o \le r, \end{cases} \tag{15}$$

and

$$s(r) = f_2(r) = \begin{cases} 0, & r \le r_i, \\ 2(r - r_i)/p\bar{r}d^2, & r_i \le r \le \bar{r}, \\ 2(r_o - r)/p\bar{r}d^2, & \bar{r} \le r \le r_o, \\ 0, & r_o \le r, \end{cases} \tag{16}$$

where $\bar{r} = (r_o + r_i)/2$ is an average beam radius and $d = r_o - r_i$ is the beam width.

In Figs. 2 and 3, we summarize our numerical results for the case of the quadratic function. Figure 2(a) is a plot of $f_1 a^2$ versus r/a for $\bar{r}/a = 0.8$ and $d/a = 0.12$, which corresponds to $r_i/a = 0.74$ and $r_o/a = 0.86$. In Fig. 2(a), f_1 has been reconstructed from 200 modes of the Bessel function expansion given by (3) and (15). The justification for the high number of modes used in this calculation is due to the convergence rate of s. The beam edges are locations of large numerical fluctuations and slower convergence, when expanding in Bessel functions. Near the beam's inner and outer radii, the electric field, given by (7), reaches its maximum and minimum, respectively. Hence, we need enough modes to sufficiently resolve Γ near the outer radius, where Γ_{max} occurs. By choosing $a = 1.0$, we plot Γ in Fig. 2(b), as obtained numerically with 200 modes.

Notice that the maximum of Γ occurs slightly less than the outer radius of the beam $(r/a \approx 0.848)$, and its value is approximately $\Gamma_{max} \approx 49.1$. From (13), we immediately conclude that our choice in the self-field parameter must satisfy, $2w_p^2/w_c^2 \le 0.0204$. If we only use 20 modes, the value of Γ_{max} is about 10% below $\Gamma_{max} \approx 49.1$, which is obtained with the 200 modes. In general, we find that the numerical results converge with 100 or more modes.

We should also note two facts about the function $\Gamma(r)$. First, as s approaches a flattop distribution near the outer radius, the maximum of Γ inside the beam will approach r_o and $\Gamma_{max} \to \infty$. Secondly, the fluctuations in Γ near $r/a = 0$ are caused by the mode expansion, and are irrelevant for the current problem, since we are only physically interested in the regime $r_i \le r \le r_o$.

Using the 200 mode expansion of $\Gamma(r)$ from Fig. 2(b) and equation (14), we plot the fast and slow branch solutions for $w_b(r)$ as a function of r/a for $2w_p^2/w_c^2 =$ 0.01, 0.015, and 0.019. The function $w_b(r)$ is plotted only in the region $r_i \le r \le r_o$. Note that the slow branch solution of $w_b(r)$ will undergo a sign reversal within the beam, whereas the fast branch will always remain positive. Also, note that at the critical value $2w_p^2/w_c^2 = 1/\Gamma_{max}$, the fast and slow branches will intersect at one point within the beam, although it is not shown explicitly in Fig. 3.

In order to have further confidence that the model is able to predict the critical self-field parameters for confinement when comparing to experiments, equation (13) should be approximately invariant for choice of $s(r)$. Hence, we compare the predicted critical self-field parameters for the two trial functions, f_1 and f_2 in (15) and (16). Figures 4(a) and 4(b) show plots of the exact f_1 and f_2 functions, respectively, for $\bar{r}/a = 0.8$ and various values $d/a =$ 0.08, 0.12, 0.16, and 0.2. Figure 5 shows a plot of the critical self-field parameter $2w_p^2/w_c^2 = 1/\Gamma_{\max}$ versus d/a for f_1 and f_2. In Fig. 5, we chose $\bar{r}/a = 0.8$ and $a = 2pa/g_b L = 1.0$. The calculated self-field parameters for the two different trial functions are nearly identical as shown in Fig. 5. The difference between the self-field parameters of the quadratic functions and their equivalent tent functions is about 1%. Notice that the critical self-field parameter for both functions decreases as d/a decreases. This behavior is intuitively obvious, since the bunches of charge are radially compressed while keeping N_b fixed; hence, the electric field will rise due to the increase in radial beam density.

IV. APPLICATION TO ANNULAR BEAM EXPERIMENTS

In this section, we will apply the bunched annular beam equilibrium theory to three experiments, namely, the 1.3 GHz RKA experiment at LANL [1], the 1.3 GHz relativistic klystron oscillator (RKO) experiment at AFRL [2], and the 9.4 GHz backward wave oscillator (BWO) experiment at the University of New Mexico [3]. All three of these experiments utilize an annular electron beam for high-power microwave generation, whose transverse size is comparable to the conductor wall. If the operating parameters of an annular beam experiment are such that equation (13) is violated, than the beam would not be in equilibrium once the beam is fully bunched during high-power operation of the experiment. Equilibrium could be achieved if the beam reduces space charge by a loss mechanism to the surrounding conducting wall, and such a mechanism is known to be a cause of microwave pulse shortening.

The motivation for comparing the RKA experiment at LANL with our theory is that this experiment reported microwave pulse shortening, as well as indications of beam loss and anomalous beam halo formation [1]. In Ref. 13, the LANL group provided an analysis of a modulated space-charge current limit due to the large potential depression for HPM sources, which they claimed may be responsible for the amount of microwave power which can be extracted in their RKA experiment. However, their current limit does not include the effect of beam confinement by magnetic focusing, and hence, does not explain the beam halo formation or the beam loss often associated with microwave pulse shortening. We will show that the RKA experiment is operating slightly above the effective self-field parameter limit in equation (13).

The other two experiments that we will examine, namely the AFRL RKO experiment [2] and the University of New Mexico BWO experiment [3], will be shown to be operating below the critical limit in (13). Although, the BWO experiment did measure beam loss it is most likely not due to the present theory (the BWO has a higher background gas pressure compared to the RKA and RKO experiments) [3]. The AFRL RKO experiment reached full beam transport without observing beam loss, which is in agreement with the current theory. The experiment did have microwave pulse length limitations that were most likely caused by rf gap voltage breakdown [2]. We have

included these experiments in our paper for the sake of comparison with the LANL RKA experiment.

We use the quadratic density function (15) to approximate the radial density distribution. The space charge limit is then numerically computed by using (13) and the relevant experimental data, which is provided in Table 1.

The parameters a and $2w_p^2/w_c^2$ can be further expressed in terms of experimental values, such as the average beam current I_b, the magnetic field B_0, the device frequency f, and the relativistic mass factor of the beam $g_b = (1 - b_b^2)^{-1/2}$. Since $v_b = fL$ and $I_b = N_b ef$, we can rewrite the dimensionless parameters a and $2w_p^2/w_c^2$ as $a = 2paf/c(g_b^2 - 1)^{1/2}$ and $2w_p^2/w_c^2 = 8c^2 I_b/w_c^2 a^2 I_A$, where $I_A = (g_b^2 - 1)^{1/2} m_e c^3/e \approx 17kA(g_b^2 - 1)^{1/2}$ is the Alfven current.

Using the experimental values from Table 1, we compare the self-field parameter, $2w_p^2/w_c^2$, for each experiment with the critical self-field parameter for the same value of a. We should note that the value of g_b chosen for modeling each of the experiments corresponds to the injected energy, i.e. $g_b = g_{inj}$, and not the value g due to space-charge depression [9], i.e.

$$(g_{inj} - g)(1 - g^{-2})^{1/2} = \frac{2I_b}{17kA} ln\left(\frac{2a}{r_i + r_o}\right). \qquad (17)$$

In the case of the LANL RKA, the difference between g_{inj} and g is approximately 6%. However, the critical result of our theory, namely the effective space-charge density limit in (13), is essentially unaffected by the choice of g_b in the typical parameter ranges for HPM sources, as we will now demonstrate.

In equation (13), we immediately see that the left-hand side is proportional to $(g_b^2 - 1)^{-1/2}$. From equation (12), we see that $\Gamma(r)$ has a factor of $(g_b^2 - 1)^{1/2}$ outside of the power series, as well as a nonlinear dependence on $(g_b^2 - 1)^{1/2}$ in each of the $coth(pj_{on}/a)$ functions. As seen from Table 1, a typical range for a is $0.5 < a < 2.0$, and hence

$coth(pj_{on}/a) \approx 1.0$ to within 0.1%. Therefore, $(g_b^2 - 1)^{1/2}$ may be factored out of equation (13) to a very good approximation, and the theory becomes invariant for choice of g_b.

For the LANL RKA experiment, $a \approx 0.54$ and $2w_p^2/w_c^2\big|_{exp} \approx 0.0133$ during the maximum current operation of 6 *kA*. Using (13), we obtain the theoretical space-charge limit of $2w_p^2/w_c^2\big|_{crit} \approx 0.0126$, which implies that the beam may not be in equilibrium. One way for the beam to reach equilibrium is by beam loss to the conductor wall, thereby reducing the value of $2w_p^2/w_c^2\big|_{exp}$ such that it equals $2w_p^2/w_c^2\big|_{crit}$. This may be the explanation of the anomalous beam halo and the consequential beam loss, which were both observed in the RKA experiment. Assuming that beam loss corresponds to the beam trying to reach bunched equilibrium as discussed in Sec. II, a simple estimate on the amount of beam current loss may be made, namely

$$\% \text{ beam current loss} = \frac{2w_p^2/w_c^2\big|_{exp} - 2w_p^2/w_c^2\big|_{crit}}{2w_p^2/w_c^2\big|_{exp}}. \qquad (18)$$

In this case, the predicted percentage of beam current loss would be about 5%. Unfortunately, the authors were not provided with experimental measurement of beam current loss with which to compare this result.

For the AFRL RKO experiment, $a \approx 1.2$ and $2w_p^2/w_c^2\big|_{\exp} \approx 0.0021$. The theoretical space-charge limit for the RKO experiment is given by $2w_p^2/w_c^2\big|_{crit} \approx 0.0161$, hence this experiment is operating well-below the space charge limit. For the University of New Mexico BWO experiment, $a \approx 1.83$ and $2w_p^2/w_c^2\big|_{\exp} \approx 0.0045$, whereas the corresponding theoretical limit is given by $2w_p^2/w_c^2\big|_{crit} \approx 0.059$. In both of these experiments, the experimental values of $2w_p^2/w_c^2$ are an order of magnitude lower than the corresponding theoretical limits for bunched annular beam confinement. This implies that if the beam reaches a bunched equilibrium, it will be well below the theoretical space-charge limit for an equilibrium to exists.

The fact that the experimental value of the self-field parameter for the BWO, $2w_p^2/w_c^2$, is significantly lower than its critical value implies that this theoretical limit is probably not the cause of the observed microwave pulse shortening and beam loss. While the density functions used for the experimental modeling are in fluid equilibrium, we have not established the stability of the equilibrium, which will be an important subject in our further investigation. Such a stability calculation will include both radial and azimuthal perturbations of the beam equilibrium in the fluid theory. If the bunched beam equilibrium is unstable, it may lead to a lower value of the self-field parameter for confinement of the bunched annular beam.

Our theory has also ignored the longitudinal component of the beam. The purpose for ignoring the longitudinal beam thickness was to simplify the theory. Our zero-thickness model, which we have developed in this paper, may be interpreted as an extreme form of a bunched beam. It produces the strongest coupling that a periodic charged beam can have to a perfectly conducting pipe, while still retaining the realistic finite transverse size. The strong beam wall coupling has the effect of reducing the critical value of $2w_p^2/w_c^2$, since a greater magnetic field is needed in order to confine the beam. However, a self-consistent theory incorporating the third dimension of the beam would have the effect of increasing the critical self-field parameter.

V. SUMMARY

We have studied the confinement of a periodic, azimuthally invariant bunched annular beam inside of a perfectly conducting cylinder in the framework of a cold-fluid equilibrium theory. In order to balance the internal repulsive electric field force of the beam, we include a uniform external magnetic focusing field. The model allows for an arbitrary transverse density profile and provides the self-consistent electric and magnetic fields due to the beam with the appropriate boundary conditions at the wall. The model also incorporates the correct relativistic effects from the longitudinal motion of the beam.

The self-consistent electric and magnetic fields in the plane of a flat bunch were analytically computed by first, expanding the density function in terms of Bessel functions, and then utilizing an electrostatic Green's function for periodic point charges. From the equilibrium force balance equation, we derived the equilibrium beam rotation and established an upper bound on the effective self-field parameter, $2\omega_p^2/\omega_c^2$, for equilibrium to exist.

In order to demonstrate the robustness of our model with regard to density profiles, we numerically found that the space charge limit for annular beams remains relatively invariant with choice of distribution function. In particular, we chose two types of functions, quadratic and tent, and showed that their corresponding critical self-field parameters only vary by a fraction of a 1%.

We have shown that the parameters for an annular beam experiment (i.e. average beam current, magnetic field strength, etc.) may used to calculate the relevant parameters in our annular beam model. In doing so, a self-consistent equilibrium fluid model for an experiment may be established. The quadratic function was used to numerically model the annular beams of three high-power microwave experiments, the LANL 1.3 GHz RKA, the AFRL 1.3 GHz RKO, and the University of New Mexico's 9.4 GHz BWO.

The LANL RKA experiment was found to be operating slightly above the critical space-charge limit for bunched beam equilibrium. Operation above the critical limit may have caused a percentage of the beam current to be lost to the wall, which in turn could lead to microwave pulse shortening.

The AFRL RKO and the University of New Mexico BWO experiments were both found to be operating well below the critical space-charge limit. This result agrees with

the successful beam transport in the AFRL RKO experiment, but does not agree with the observed beam loss and microwave pulse shortening in the UNM BWO experiment. While the bunched annular beam in the BWO experiment is well confined from the viewpoint of an equilibrium theory, the stability of the bunched beam equilibria remains to be determined in order to answer the question of whether or not beam loss occurs in this experiment. This will be an important subject for further investigation.

ACKNOWLEDGEMENTS

This work was supported by the Air Force Office of Scientific Research, Grant No. F49620-00-1-0007, and by the Department of Energy, Office of High Energy and Nuclear Physics, Grant No. DE-FG02-95ER-40919.

APPENDIX A: DERIVATION OF THE SELF-FIELDS

The equilibrium self-electric and self-magnetic fields, $E^{self}(r)\hat{\mathbf{e}}_r$ and $B^{self}(r)\hat{\mathbf{e}}_q$, are found by calculating them in the rest frame of the beam and then performing a Lorentz transformation back to the laboratory frame. The advantage of this approach is that in the beam rest frame, the self-magnetic field is negligibly small. Therefore, it is sufficient to calculate only the self-electric field of the beam including the full effect of induced charge on the conducting cylinder. Indeed, by introducing the scalar and vector potentials, $f^{self}(r)$ and $A^{self}(r)\hat{\mathbf{e}}_z$ in the laboratory frame, and correspondingly $f^{self}_{rest}(r)$ and $\mathbf{A}^{self}_{rest}(r)$ in the rest frame, it is readily shown from the Lorentz transformation that

$$f^{self}(r) \cong g_b f^{self}_{rest}(r) \tag{A1}$$

and

$$A^{self}(r)\hat{\mathbf{e}}_z \cong g_b b_b f^{self}_{rest}(r)\hat{\mathbf{e}}_z \tag{A2}$$

where $b_b = V_z/c$ and use has been made of the approximation $\mathbf{A}^{self}_{rest}(r) = 0$. From the definitions for the scalar and vector potentials, the self-electric and self-magnetic fields are given by

$$\mathbf{E}^{self}(r) = -\hat{\mathbf{e}}_r g_b \frac{\partial f^{self}_{rest}(r)}{\partial r} = g_b E^{self}_{rest}(r)\hat{\mathbf{e}}_r \tag{A3}$$

$$\mathbf{B}^{self}(r) = -\hat{\mathbf{e}}_q g_b b_b \frac{\partial f^{self}_{rest}(r)}{\partial r} = -g_b b_b E^{self}_{rest}(r)\hat{\mathbf{e}}_q \tag{A4}$$

An electrostatic Green's function technique, which was utilized in a recent work on bunched beams [4], is used to calculate the scalar potential $f^{self}_{rest}(r)$ and self-electric field $E^{self}_{rest}(r)\hat{\mathbf{e}}_r$ in the rest frame of the beam. Specifically, for a periodic collinear distribution of unit point charges separated by a distance $L_{rest} = g_b L$ inside of a perfectly conducting cylinder of radius *a*, the electrostatic Green's function satisfies the following two equations in the rest frame of the beam,

$$\nabla^2 G(\mathbf{r};\mathbf{r}') = -4p \sum_{k=-\infty}^{\infty} d(\mathbf{r} - \mathbf{r}' - kL_{rest}\hat{\mathbf{e}}_z) \tag{A5}$$

and

$$G(\mathbf{r};\mathbf{r}')\big|_{r=a} = 0 \tag{A6}$$

where $\mathbf{r}$ and $\mathbf{r}'$ are the coordinates of the point of observation and the location of a point charge, respectively. The solution to equations (A5) and (A6) is given by [4]

$$G(\mathbf{r};\mathbf{r}') = \frac{1}{L_{rest}} ln\left[\frac{a^2 + r_>^2 r_<^2/a^2 - 2r_> r_< cos[q-q']}{r_>^2 + r_<^2 - 2r_> r_< cos[q-q']}\right] + \frac{4}{L_{rest}} \sum_{l=-\infty}^{\infty}\sum_{k=1}^{\infty} cos[l(q-q')]cos[k(\hat{z}-\hat{z}')]\frac{I_l(k\hat{r}_<)}{I_l(ka)}[I_l(ka)K_l(k\hat{r}_>) - K_l(ka)I_l(k\hat{r}_>)], \quad \text{(A7)}$$

where $r_>(r_<)$ denotes the greater (lesser) of r and r', $I_l(x)$ and $K_l(x)$ are the *l*th order modified Bessel functions of the first and second kind, respectively, $a = 2pa/L_{rest}$, and hat '^' denotes normalization by $2p/L_{rest}$.

The electrostatic self-potential $f_{rest}^{self}(\mathbf{r})$ may be found from Coulomb's Law,

$$\nabla^2 f_{rest}^{self}(\mathbf{r}) = 4peN_b s(r)\sum_{k=-\infty}^{\infty} d(z - kL_{rest}) \quad \text{(A8)}$$

with the boundary condition at the conductor wall,

$$f_{rest}^{self}(\mathbf{r})\Big|_{r=a} = 0. \quad \text{(A9)}$$

By utilizing the electrostatic Green's function (A7), we can find that the electrostatic potential in the plane of the beam, i.e., $f_{rest}^{self}(r) = f_{rest}^{self}(\mathbf{r})\Big|_{z=z'=0}$, can be expressed as

$$f_{rest}^{self}(r) = -N_b e \lim_{\Delta r \to 0} \int_0^{2p} dq' \left[\int_0^{r-\Delta r} dr' r' s(r') G(\mathbf{r};\mathbf{r}')\Big|_{z=z'} + \int_{r+\Delta r}^{a} dr' r' s(r') G(\mathbf{r};\mathbf{r}')\Big|_{z=z'}\right]. \quad \text{(A10)}$$

In (A10), the radial integral must be split into two parts, namely $r' < r$ and $r' > r$, in order to ensure convergence of $f_{rest}^{self}(r)$. In mathematical formalism, $f_{rest}^{self}(r)$ is obtained by taking the principal integral of $r's(r')G(\mathbf{r};\mathbf{r}')$ in the radial direction. Using the azimuthal symmetry assumption and the relation, $\int_0^{2p} dq' \ln[x^2 + y^2 - 2xy\cos(q-q')] = 4p \ln x$ for $0 \le y < x$ [14], we find,

$$f_{rest}^{self}(r) = -N_b e \lim_{\Delta r \to 0}\left[\int_0^{r-\Delta r} dr' r' s(r') F(r;r') + \int_{r+\Delta r}^{a} dr' r' s(r') F(r;r')\right], \quad \text{(A11)}$$

where

$$F(r;r') = \frac{4p}{L_{rest}} \ln\left[\frac{a}{r_>}\right] + \frac{8p}{L_{rest}} \sum_{k=1}^{\infty} \frac{I_0(k\hat{r}_<)}{I_0(ka)} \left[I_0(ka) K_0(k\hat{r}_>) - K_0(ka) I_0(k\hat{r}_>)\right]. \quad \text{(A12)}$$

Hence,

$$\begin{aligned} E^{self}(r) = -\frac{4pN_b g_b e}{L_{rest}} \Bigg[& \frac{1}{r} \int_0^r dr' r' s(r') + \frac{4p}{L_{rest}} \sum_{k=1}^{\infty} \frac{k I_1(k\hat{r}) K_0(ka)}{I_0(ka)} \int_0^a dr' r' s(r') I_0(k\hat{r}') \\ & + \frac{4p}{L_{rest}} \lim_{\Delta r \to 0} \left\{ \sum_{k=1}^{\infty} k K_1(k\hat{r}) \int_0^{r-\Delta r} dr' r' s(r') I_0(k\hat{r}') - \sum_{k=1}^{\infty} k I_1(k\hat{r}) \int_{r+\Delta r}^{a} dr' r' s(r') K_0(k\hat{r}') \right\} \Bigg] \end{aligned} \quad \text{(A13)}$$

Note that the first term on the right hand side of (A13) represents the electric field due to a longitudinally uniform beam and the other three terms are the corrections due to the longitudinal bunching of the beam. Utilizing the density expansion given in (3), the following Bessel function integrals [15],

$$\begin{aligned} & \int_0^1 dx x J_0(yx) = y^{-1} J_1(y), \\ & \int_0^1 dx x J_0(yx) I_0(zx) = \left(y^2 + z^2\right)^{-1} \left[z J_0(y) I_1(z) + y J_1(y) I_0(z)\right], \\ & \int_w^1 dx x J_0(yx) K_0(zx) = \left(y^2 + z^2\right)^{-1} \left[y J_1(y) K_0(z) - z J_0(y) K_1(z) \right. \\ & \qquad \left. + zw J_0(yw) K_1(zw) - yw J_1(yw) K_0(zw)\right], \end{aligned} \quad \text{(A14)}$$

and the Wronskian relation, $I_0(x)K_1(x) + I_1(x)K_0(x) = 1/x$, we obtain the following form for the electric self-field

$$E^{self}(r) = -\frac{4pN_b ea}{L} \left[\sum_{m=1}^{\infty} \frac{s_m}{j_{0m}} J_1(j_{0m} r/a) + 2 \sum_{m=1}^{\infty} \sum_{k=1}^{\infty} \frac{s_m j_{0m}}{j_{0m}^2 + k^2 a^2} J_1(j_{0m} r/a) \right]. \quad \text{(A15)}$$

A further simplification is made by employing the relation [16] $\sum_{k=1}^{\infty} \left(y^2 + k^2 x^2\right)^{-1} = p \coth(py/x)/2yx - 1/2y^2$, which yields

$$E^{self}(r) = -2pN_b e g_b \sum_{m=1}^{\infty} s_m J_1(j_{0m} r/a) \coth(j_{0m} g_b L/2a). \quad \text{(A16)}$$

This concludes the derivation of (7) and (8) in Sec. II.

REFERENCES

[1]M.V. Fazio, W.B. Haynes, B.E. Carlsten, and R.M. Stringfield, IEEE Trans. Plasma Sci. **22**, 740 (1994).

[2]K.J. Hendricks, P.D. Coleman, R.W. Lemke, M.J. Arman, and L. Bowers, Phys. Rev. Lett. **76**, 154 (1996).

[3]F. Hegeler., C. Grabowski., and E. Schamiloglu, IEEE Trans. Plasma Sci. **26**, 275 (1998).

[4]M. Hess and C. Chen, Phys. Plasmas **7**, 5206 (2000).

[5]M. Hess and C. Chen, "Beam Confinement in Periodic Permanent Magnet Focusing Klystrons", submitted for publication in Physics Letters A, (2001).

[6]D. Sprehn, G. Caryotakis, E. Jongewaard, and R. M. Phillips, in *Proceedings of the 19th International Linac Conference*, Argonne National Laboratory Report, (1998), p. 689.

[7]D. Sprehn, G. Caryotakis, E. Jongewaard, R. M. Phillips, and A. Vlieks, in *Intense Microwave Pulses VII*, edited by H.E. Brandt, SPIE Proc. **4301**, 132 (2000).

[8]G. Scheitrum, private communication, (2000).

[9]See, for example, R.C. Davidson, *Physics of Nonneutral Plasmas* (Addison-Wesley, Reading, MA 1990), Chap. 9.

[10]S. A. Prasad and G. J. Morales, Phys. Fluids **30**, 3475 (1987).

[11]S. A. Prasad and G. J. Morales, Phys. Fluids B **1**, 1329 (1989).

[12]See, for example, Ref. 9, Chap. 6.

[13]B.E. Carlsten, R.J. Faehl, M.V. Fazio, W.B. Haynes, and R.M. Stringfield, IEEE Trans. Plasma Sci. **22**, 719 (1994).

[14]I. S. Gradshteyn and I. M. Ryzhik, *Table of Integrals, Series, and Products*, Fifth Edition, (Academic, London, 1994), p. 560.

[15]G.N. Watson, *A Treatise on the Theory of Bessel Functions*, (Cambridge University, Cambridge, 1980), pp. 132-134.

[16]V. Mangulis, *Handbook of Series for Scientists and Engineers*, (Academic, New York, 1965), p. 26.

FIGURE CAPTIONS

Fig. 1. Schematic of periodic bunched annular disks inside of a perfectly conducting drift tube.

Fig. 2. Plots of (a) quadratic beam density function versus normalized radius for an annular beam centered at *r/a=0.8*, (b) Γ versus normalized radius for the annular beam in (a). Here, 200 eigenmodes are used in the calculation.

Fig. 3. The fast (top of graph) and slow (bottom of graph) branches of $w_b(r)$ in the region $r_i \le r \le r_o$ corresponding to the 200 mode expansion of $\Gamma(r)$ in Fig. 2(b) for three different values of $2w_p^2/w_c^2$ = *0.01* (solid lines), *0.015* (dashed lines), and *0.019* (dotted lines).

Fig. 4. Plots of (a) quadratic and (b) tent beam density functions versus normalized radius for several bunched annular beams centered at *r/a=0.8*.

Fig. 5. Plots of $2w_p^2/w_c^2$ versus normalized annular beam width for quadratic and tent density functions centered at *r/a=0.8*.

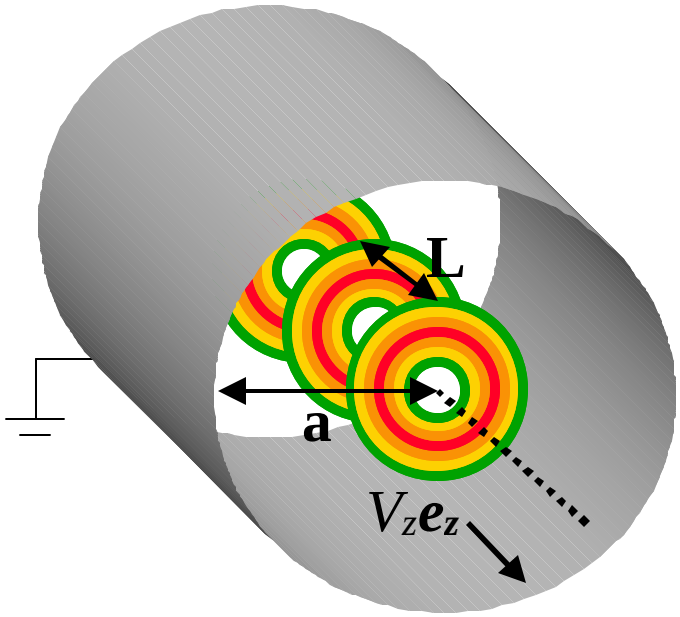

Figure 1

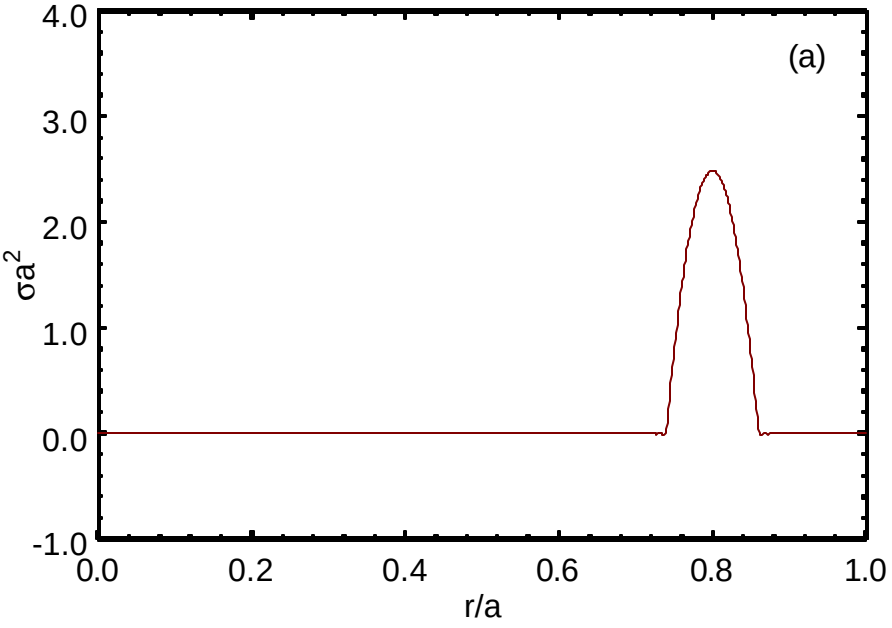

Figure 2(a)

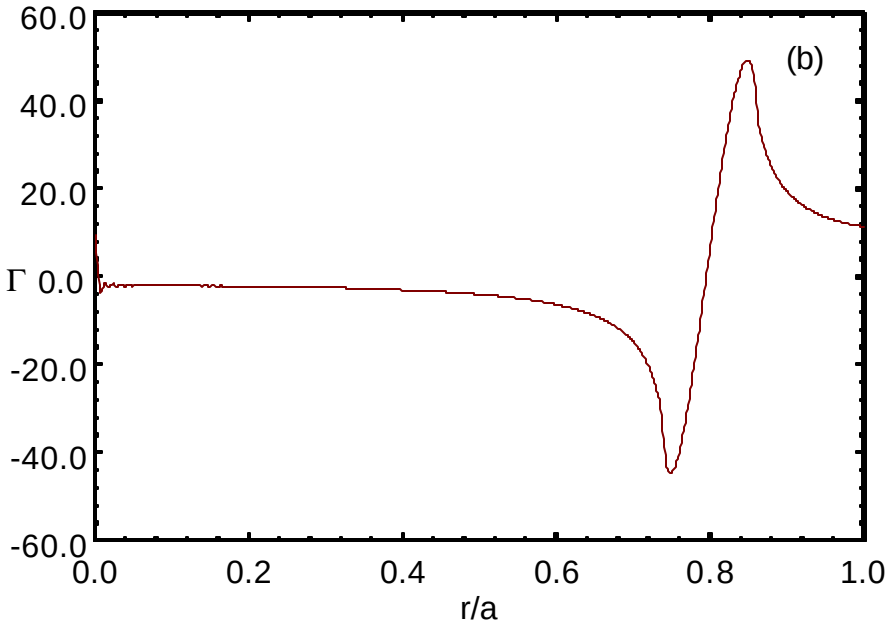

Figure 2(b)

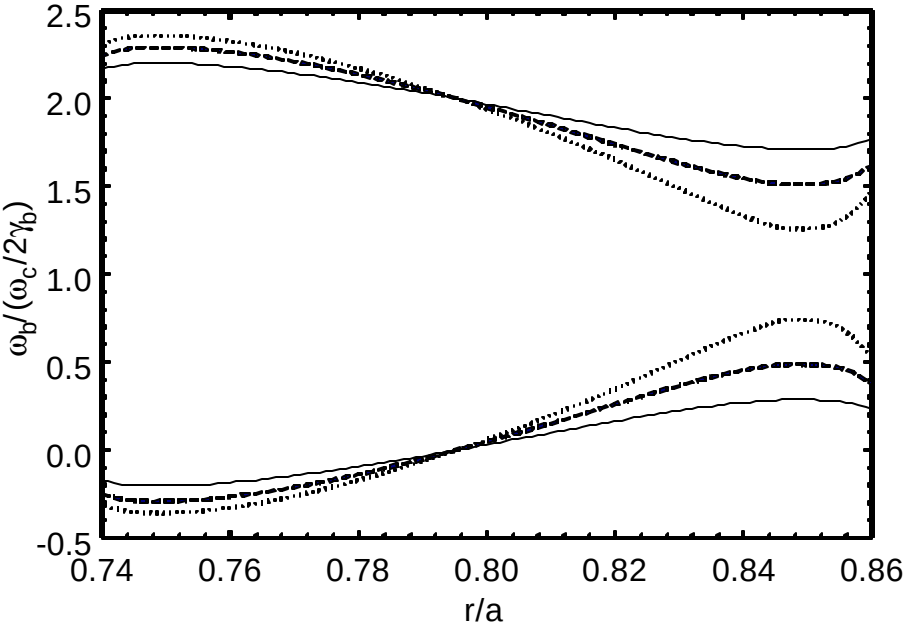
2.5
2.0
1.5
1.0
0.5
0.0
-0.5
$\omega_b/(\omega_c/2\gamma_b)$
0.74
0.76
0.78
0.80
0.82
0.84
0.86
r/a

Figure 3

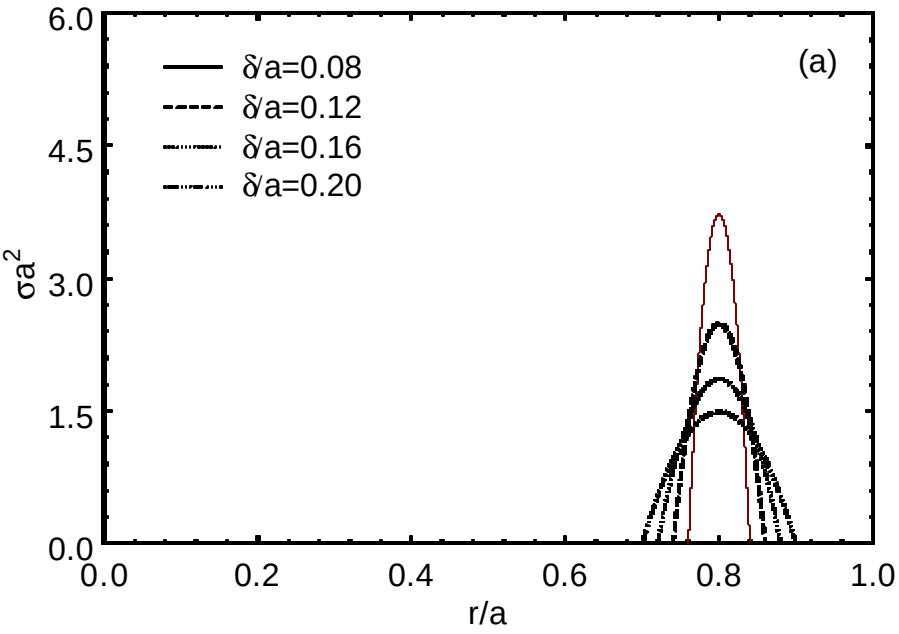

Figure 4(a)

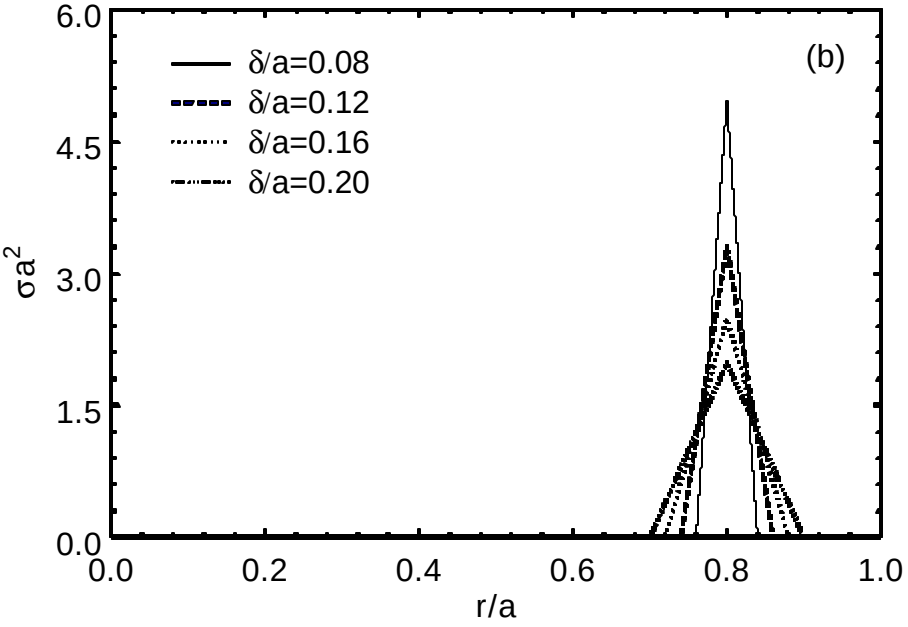

Figure 4(b)

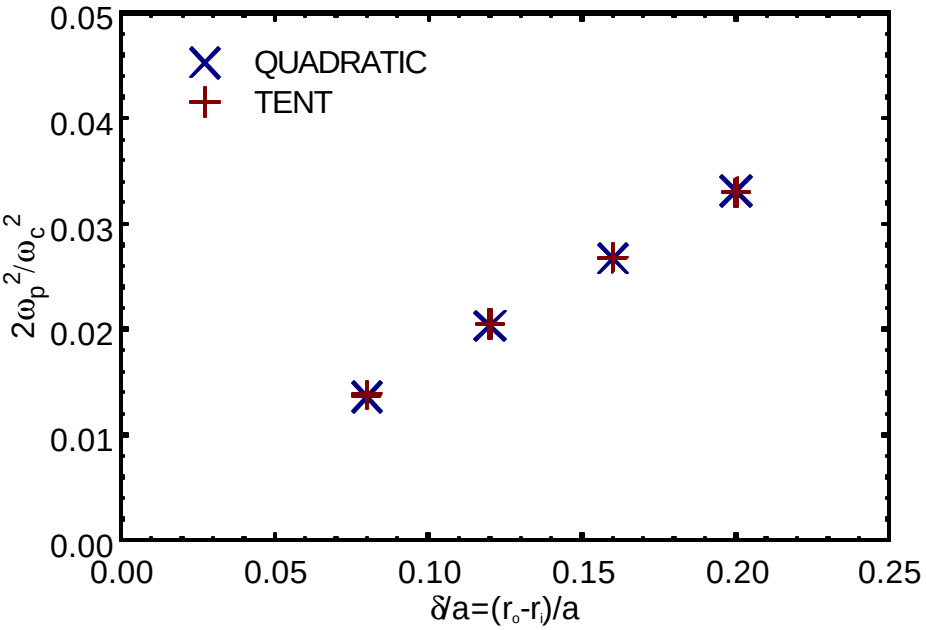
QUADRATIC
TENT
0.05
0.04
0.03
0.02
0.01
0.00
0.00
0.05
0.10
0.15
0.20
0.25
$2\omega_p^2/\omega_c^2$
$\delta/a=(r_o-r_i)/a$

Figure 5

Table 1. Parameters of Three Annular Beam HPM Devices

PARAMETER	**RKA**	**RKO**	**BWO**
f (GHz)	1.3	1.3	9.4
I_b (kA)	6.0	10.0	3.0
g_b	2.1	2.0	1.7
B_0 (T)	0.5	0.8	2.0
r_i (cm)	2.70	6.60	0.90
r_o (cm)	3.20	7.10	1.15
a (cm)	3.65	7.65	1.28
a	0.54	1.20	1.83
$\left.\frac{8c^2 I_b}{w_{c,rms}^2 a^2 I_A}\right\|_{exp}$	0.0133	0.0021	0.0045
$\left.\frac{8c^2 I_b}{w_{c,rms}^2 a^2 I_A}\right\|_{cr}$	0.0126	0.016	0.059